Attenuation of Millimeter-Wave in a Sand and Dust Storm

Mu-Min Chiou and Jean-Fu Kiang

***Abstract*—The attenuation of millimeter-wave signals in a sand and dust storm (SDS) can be used to retrieve SDS parameters. A parabolic wave equation method is proposed to simulate millimeter-wave propagation in an SDS, including the effects of absorption and Rayleigh scattering by dust particles with given height profiles of particle-size distribution and total number density. Three different aperture fields of the transmitting antenna are also chosen to simulate wave attenuation under different sets of SDS parameters.**

***Index Terms*— Attenuation, millimeter wave, parabolic wave equation (PWE), Rayleigh scattering, sand and dust storm (SDS).**

I. Introduction

SAND and dust storms (SDSs) are frequently observed in many areas around the world [1], [2], which may cause pollution, respiratory diseases, ecological disaster, low visibility, and interrupted traffic [3]. Some of these impacts can be prevented if the dust storms can be monitored in real time, for example, by conducting Moderate Resolution Imaging Spectroradiometer (MODIS) solar reflectance band measurements [2]. The potential effects of SDSs on the atmosphere have been studied by using multiple satellite remote sensing data sets and meteorological information [4]. Various satellite-based techniques were also proposed for monitoring dust storms [3]–[8].

Spaceborne observations can provide global coverage of SDSs, whereas ground-based observations can provide more detailed information [1]. For example, MODIS is capable of sensing the Earth surface at nadir with a minimal vertical resolution of 250 m, which may not be fine enough to probe an SDS that typically stays below 100 m above the ground, and the height distribution of atmospherical parameters within this thin layer vary over quite a wide range [5]. Typical parameters of an SDS, including visibility, total number density, particle size distribution, and land surface coverage [3], also significantly vary within this layer.

Wireless sensor networks (WSNs) have been extensively used for monitoring natural hazards such as volcanic eruption, earthquake, and flood. A WSN can be deployed in a specific area to collect real-time data for tracking the origin of dusts [9], but more field trials and algorithms are required to make it practical. The attenuation, phase shift, and fluctuations of microwave and millimeter-wave signals propagating through an SDS have been studied [10], [11], including the effects of total number density, particle size distribution, and particle shape.

From field measurements, it was found that the distributions of total number density and particle size within an SDS were strong functions of height [12], [13]. A parabolic wave equation (PWE) method, suitable for simulating wave propagation in the lower atmosphere [14], [15], will be applied to study the effects of an SDS with height-dependent distributions.

Before retrieving SDS parameters from the attenuation of millimeter-wave signals, it will be useful to study the forward problem of wave propagation through SDSs with different distributions. In this letter, a conventional PWE method will be modified by including the effects of absorption and Rayleigh scattering from dust particles in an SDS with height profiles of total number density and size distribution. The absorption by air and water vapor in the atmosphere is also included, and three different aperture field distributions of the transmitting antenna will be compared for their effectiveness in achieving more accurate predictions.

This letter is organized as follows. The attenuation due to Rayleigh scattering is presented in Section II, the effects of SDS parameters on attenuation is presented in Section III, the proposed method is presented in Section IV, and the simulations are discussed in Section V. Finally, some conclusions are drawn in Section VI.

II. Attenuation Due to Rayleigh Scattering

The propagation constant of a plane wave in an atmosphere filled with dust particles can be represented as [16], [17]

$$k_v(\bar{r}) = k_0 + \frac{2\pi}{k_0} N_t(\bar{r}) \int_0^{r_{p\max}} P(\bar{r}, r_p) f_v(r_p) dr_p \qquad (1)$$

where k_0 is the wavenumber in free space; $N_t(\bar{r})$ (in m^{-3}) is the total number density of dusts; r_p is the radius of a dust particle, with the probability density function of $P(\bar{r}, r_p)$ $(1/\mu\mathrm{m/m}^3)$; and f_v is the forward scattering amplitude with vertical polarization. The radius of a dust particle is typically below 100 μm [13], and a maximum value of $r_{p\max} = 150$ μm [10] is assumed in this letter.

The dust particles are approximately of spherical shape, and their radii are much smaller than one wavelength; hence, the

Manuscript received December 5, 2015; revised April 4, 2016; accepted May 7, 2016. Date of publication May 31, 2016; date of current version July 20, 2016. This work was supported by the Ministry of Education, Taiwan, under Project 103R3401-1.

The authors are with the Department of Electrical Engineering and the Graduate Institute of Communication Engineering, National Taiwan University, Taipei 10617, Taiwan (e-mail: jfkiang@ntu.edu.tw).

Color versions of one or more of the figures in this letter are available online at http://ieeexplore.ieee.org.

Digital Object Identifier 10.1109/LGRS.2016.2566799

forward scattering amplitude of Rayleigh approximation can be applied, which is [16]

$$f_v = \frac{\epsilon_d - 1}{\epsilon_d + 2} k_0^2 r_p^3 \tag{2}$$

where ϵ_d is the relative permittivity of dust material, which depends on the sand composition, wave frequency, and the environmental moisture.

III. Effects of SDS Parameters on Attenuation

The height profile of the total number density of dust particles can be approximated by [12]

$$N_t = N_{ts} z^{-\Gamma_p} \tag{3}$$

where N_{ts} is the total number density at 1 m above the ground, and the index Γ_p depends on particle sedimentation and frictional velocity, which is typically larger than 0.29 [13].

The size distribution of dust particles in an SDS can be characterized with a lognormal distribution [13], where the mean and the standard deviation of radii can be derived by fitting the measurement data. The average particle radius r_0 can be estimated as [13]

$$r_0 = r_{0s} z^{-\gamma_m} \tag{4}$$

where r_{0s} is the average particle radius at 1 m above the ground. The standard deviation of particle radius is assumed to follow the same height profile of r_0, i.e.,

$$\sigma_p = \sigma_{ps} z^{-\gamma_\sigma}. \tag{5}$$

The specific attenuation constant (in decibels/kilometer), phase shift constant (in radians per meter), and refractivity of waves in an SDS can be then determined by

$$\alpha_{\text{ds}} = 8686 \times \text{Im}\{k_v\} \tag{6}$$

$$\beta_{\text{ds}} = \text{Re}\{k_v\} \tag{7}$$

$$n_{\text{ds}} = k_v / k_0 \tag{8}$$

where n_{ds} is the refractivity index attributed to SDS, and $k_v(\bar{r})$ is determined from (1).

Fig. 1 shows the specific attenuation constant α_{ds} and the imaginary part of refractivity N''_{ds}, respectively, of waves at $f = 100$ GHz, attributed to SDS. It is assumed that the total number density follows the height profile in (3) and the average value and standard deviation of particle radius follow the height profiles in (4) and (5), respectively, with $\gamma_m = 0.15$ and $\gamma_\sigma = 0.1245$, which are derived by fitting the measurement data listed in Table I [13]. The total number density at 1 m above the ground is chosen to be $N_{ts} = 5 \times 10^7$, representing a severe SDS with visibilities of 1.4 and 4.2 m at heights of 1 and 10 m, respectively, where the visibility is related to the particle distribution as [17]

$$V_b = \left(\frac{4\pi}{3} N_t \int_0^{r_{\max}} P(r_p) r_p^3 dr_p / 9.43 \times 10^{-9} \right)^{-1.07} \text{(km)}.$$

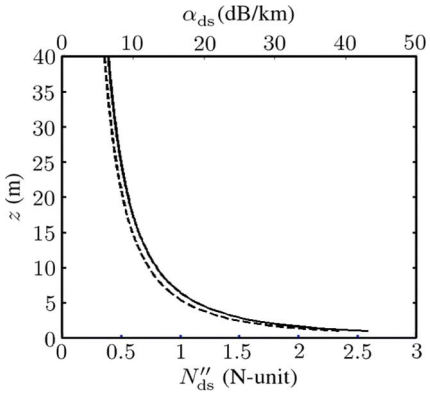

Fig. 1. Height profiles of (solid line) specific attenuation constant α_{ds} and (dash line) N''_{ds}; $f = 100$ GHz, $N_{ts} = 5 \times 10^7$, and $\epsilon_d = 3.5 - j1.64$ [10].

TABLE I
Parameters of Dust Size Distribution [13]

height (m)	mean of $\ln\{r_p\}$	standard deviation of $\ln\{r_p\}$
1	14.0	13
15	9.8	10.3
21	9.2	8.9

r_p is in unit of μm.

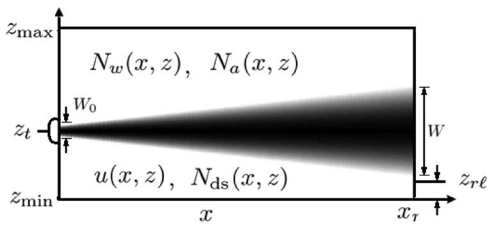

Fig. 2. Schematic of millimeter-wave propagation in an SDS.

As shown in Fig. 1, α and N''_{ds} significantly decrease from the ground level upward, implying that the height profiles of SDS parameters are significant in modeling wave propagation in an SDS.

IV. Simulation Method

Fig. 2 shows the schematic of millimeter-wave propagation in an SDS, where z_t is the height of the transmitting antenna; x_r is the range of the receiving antenna; $z_{\min}$ and $z_{\max}$ are the minimum and the maximum heights, respectively, of the computational domain. The beamwidth tends to increase from W_0 at $x = 0$ to W in the receiving plane.

To apply the PWE method, the propagating wave is first represented as $e^{-jk_0 x} u(x,z)$, where $u(x,z)$ is called the reduced amplitude function [14]. In this letter, the vertically polarized wave is considered, which is modeled as $H_y = e^{-jk_0 x} u(x,z)$. Next, the reduced amplitude function is marched in the x-direction by applying the Fourier split-step algorithm as [14]

$$u(x + \Delta x, z) = e^{-jk_0 m \Delta x/2} \mathcal{F}^{-1} \left\{ \mathcal{F}\{u(x,z)\} e^{\frac{jp^2}{(2k_0)\Delta x}} \right\} \tag{9}$$

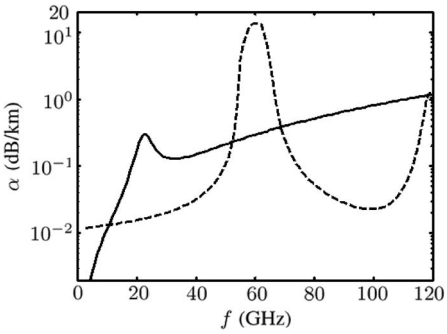

Fig. 3. Specific attenuation attributed to (dash line) dry air [18] and (solid line) water vapor [18].

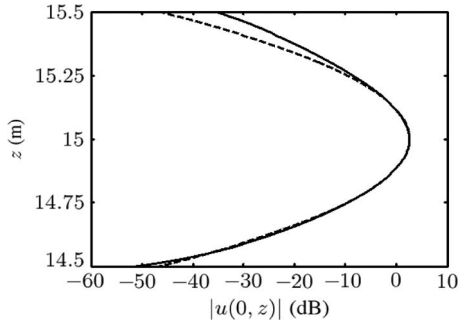

Fig. 4. Magnitude of the aperture field on the transmitting antenna. (Solid line) Parabolic reflector with feeding horn; $D = 1.2$ m and $F = 0.3$ m. (Dash line) Gaussian beam with $W_0 = 0.22$ m.

where $\mathcal{F}$ and $\mathcal{F}^{-1}$ represent the Fourier transform and the inverse Fourier transform, respectively; $p = k \sin\theta$, where θ is the propagation angle measured from the horizontal direction; and $m = n_{\rm ds}^2 - 1 + 2z/r_e$ is the modified refractive index that includes the effect of Earth curvature, where r_e is the Earth radius. The ground reflection is included, and an absorbing layer is placed on top of $z_{\max}$ to reduce artificial reflection [14].

Once the field within the computational domain is obtained, a propagation factor (PF) is determined as [14]

$$\text{PF} = 20\log_{10}|u| + 10\log_{10} x + 10\log_{10}\lambda \ (\text{dB}) \qquad (10)$$

which is the field attenuation with respect to free space.

To include atmospheric absorption, empirical formulas of refractivity attributed to air and water vapor [18] are used. Fig. 3 shows the specific attenuation constants from 3 to 120 GHz, attributed to dry air and water vapor, respectively, at the temperature of 27 °C, a relative humidity of 50%, and a pressure of 1 atm on the ground [18]. Three peaks are observed around 22, 60, and 118 GHz, respectively, which are dominated by water vapor and dry air.

Represent the refractivities attributed to water vapor and dry air as $N_w = N_w' - jN_w''$ and $N_a = N_a' - jN_a''$, respectively, where the imaginary parts account for the absorption effects. To minimize the atmospheric attenuation, the operating frequency is set to 100 GHz. At heights from 1 to 40 m in an SDS, N_w'' and N_a'' at $f = 100$ GHz are relatively smaller than $N_{\rm ds}''$. For example, in the standard atmosphere aforementioned in the last paragraph, N_w'' decreases from 0.044 to 0.042 (N-unit) and N_a'' decreases from 1.25×10^{-3} to 1.15×10^{-3} (N-unit) as the height increases from 1 to 40 m. Both are smaller than $N_{\rm ds}''$, as shown in Fig. 1.

V. Simulations and Discussions

In this letter, the aperture field of a parabolic reflector will be used as the initial field in applying the PWE method. The parabolic reflector is assumed to be axisymmetrical, with diameter D and focal length F, and an offset horn antenna pointing at the apex of the reflector is used as the feeding source.

Fig. 4 shows the aperture field on the parabolic reflector of the transmitting antenna, with $D = 1.2$ m and $F = 0.3$ m. A Gaussian beam with beamwidth $W_0 = 0.22$ m, commonly used in the PWE method, is also shown for comparison. After propagating over a distance of 1 km, the PFs of these two aperture fields differ by about 0.2 dB near the beam center and about 0.5 dB away from the beam center.

TABLE II
Three Aperture Fields for Simulation

case	F (m)	D(m)	x_r(km)
1	0.25	1	3
2	0.45	2	3
3	0.25	1	0.5

$z_t = 10$ m, $f = 100$ GHz.

Next, we will simulate and compare the PFs associated with three aperture fields listed in Table II. The transmitting antenna is located at 10 m above ground. The SDS parameters of the SDS are the same as those used to generate Fig. 1.

Fig. 5(a) shows the height profile of $\text{PF}_{\rm ds}$ at $x_r = 3$ km when the first aperture field propagates in the SDS. Due to the Earth curvature and stronger attenuation at lower altitudes, the beam center is bent upward to $z = 18$ m at $x_r = 3$ km. The difference between $\text{PF}_{\rm df}$ (when the SDS is absent) and $\text{PF}_{\rm ds}$ is also shown. It is observed that the wave is attenuated more seriously at lower altitudes where the number density of particles is higher. The fluctuations of PF difference near the ground level are caused by ground reflection, which is on the order of 0.5–5 dB below 10 m.

Fig. 5(b) shows the height profile of $\text{PF}_{\rm ds}$ and the PF difference, respectively, at $x_r = 3$ km when the second aperture field, with parameters listed in case 2 in Table II, is propagated. The fluctuations of PF difference are weaker than those shown in Fig. 5(a) because the directivity of the parabolic reflector is higher than that in case 1.

The third aperture field in Table II represents a millimeter-wave link over a relatively short path, and Fig. 5(c) shows the height profiles of $\text{PF}_{\rm ds}$ and the PF difference, respectively. It is observed that the PF difference increases from 6.1 to 7.6 dB as the receiving height is decreased from 14 to 5 m. Ground reflection is less significant above 7 m. The fluctuations above 14 m are attributed to diffraction and can be neglected because the PF therein is 15 dB smaller than the peak value.

To avoid ground reflection, the receiving antenna should be placed higher than a certain threshold, labeled $z_{r\ell}$, which is defined as the height where the fluctuation of field, as shown in Fig. 2, exceeds a specified level, i.e., $\delta_{\rm PF}$.

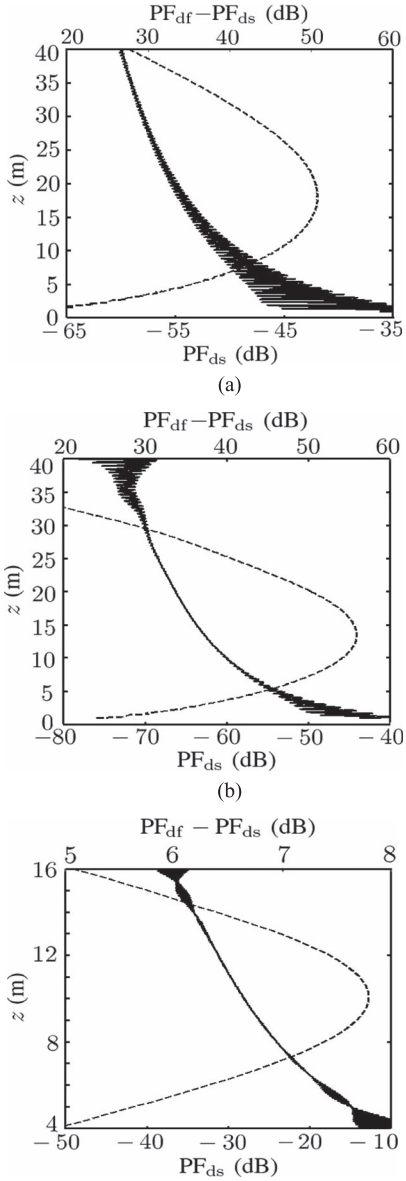

Fig. 5. (a) PF at $x_r = 3$ km in case 1 in Table II. (b) PF at $x_r = 3$ km in case 2 in Table II. (c) PF at $x_r = 0.5$ km in case 3 in Table II. (Solid line) PF$_{df}$−PF$_{ds}$. (Dash line) PF$_{ds}$.

Fig. 6 shows the lowest height $z_{r\ell}$ versus the transmitting antenna height z_t in three different cases. In the gray area ($z_{r\ell} \geq z_t$), the wave will be strongly affected by ground reflection. The fluctuation threshold is arbitrarily set to $\delta_{\text{PF}} = 0.2$ dB. In case 1 in Table II, the fluctuations at the receiving site are greater than 0.2 dB at any height of $x_r = 3$ km. Hence, x_r is reduced to 1.5 km, creating case 1′, in which $z_{r\ell}$ decreases from 7 to 2.8 m as z_t is increased from 7 to 20 m. Similarly, $z_{r\ell}$ decreases from 9.5 to 5.6 m as z_t is increased from 9.5 to 20 m in case 2, and $z_{r\ell}$ decreases from 9 to 4.7 m as z_t is increased from 9 to 20 m in case 3. By considering the tradeoff between antenna directivity and operational convenience, a moderate-size reflector is suggested, and the transmitting antenna should not be too far away from the receiving antenna.

Fig. 7 shows the PF difference (PF$_{df}$ − PF$_{ds}$) computed with the PWE method and two other height profiles of attenuation,

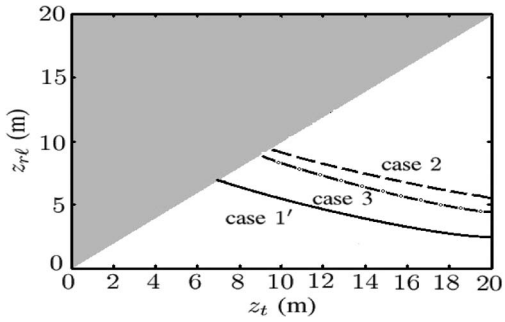

Fig. 6. Lowest receiving height ($z_{r\ell}$) versus transmitting antenna height (z_t) with $\delta_{\text{PF}} = 0.2$ dB. (Solid line) Case 1′, $F = 0.25$ m, $D = 1$ m, and $x_r = 1.5$ km. (Dash line) Case 2. (Dash-dotted line) Case 3.

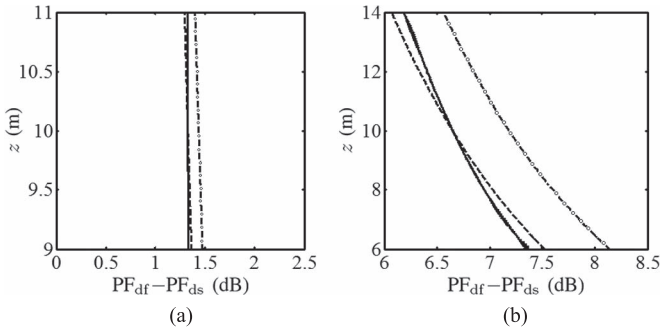

Fig. 7. Height profile of PF$_{df}$−PF$_{ds}$ in case 3 (a) at $x_r = 0.1$ km and (b) at $x_r = 0.5$ km. (Solid line) PWE method. (Dash line) Formula in [10]. (Dash-dotted line) Formula in [13].

with the specific attenuation constants derived from [13] and [10], respectively. The formula in [13] was based on a measured probability density function and Mie scattering theory, which predicted higher attenuation than measurement [17]. The formula in [10] was based on a mixing formula, and its prediction matches with that in (1) [17]. The deviation of the PF difference between the PWE method and the other two formulas increases with the propagation range. At $x_r = 0.5$ km, the slope of PF difference versus height, with $6 < z < 14$ m, predicted with the PWE method is different from those with the other two formulas, which may be attributed to the diffraction effects accounted for in the proposed PWE method.

Finally, we will briefly study the effects of SDS parameters on the PF difference. The SDS parameters used to generate Fig. 1 will be used as default. Fig. 8 shows the PF differences at three different total number densities. A larger N_{ts} implies more absorption, leading to a stronger attenuation.

Fig. 9 shows the PF differences at three different Γ_p's, which characterize the number density profile represented in (3). A larger Γ_p implies that more dust particles hover near ground and fewer particles will fall in the wave beam, leading to a smaller attenuation in the millimeter-wave signals.

We also simulate the PF difference at three different standard deviations of lognormal distribution for particle size, $\sigma_p = 12$, 13, and 14 μm, respectively. A larger σ_p implies a wider range of dust particle size or more particles with larger radii, leading to a stronger attenuation. However, the difference is well below 0.3 dB.

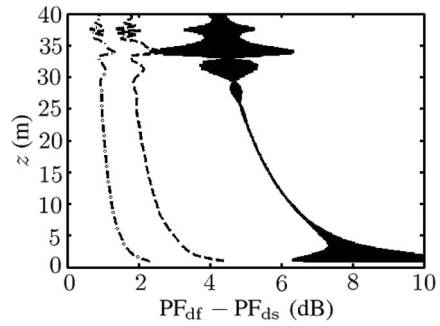

Fig. 8. $PF_{df}-PF_{ds}$ in case 3. (Dash-dotted line) $N_{ts} = 10^7$ (m^{-3}). (Dash line) $N_{ts} = 2 \times 10^7$ (m^{-3}). (Solid line) $N_{ts} = 5 \times 10^7$ (m^{-3}).

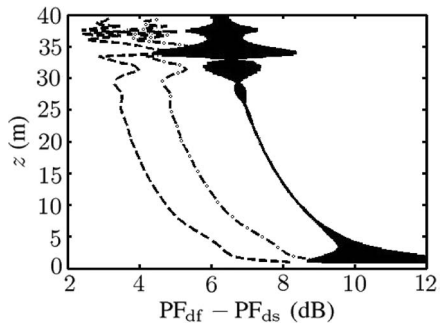

Fig. 9. $PF_{df}-PF_{ds}$ in case 3. (Dash-dotted line) $\Gamma_p = 0.29$. (Dash line) $\Gamma_p = 0.4$. (Solid line) $\Gamma_p = 0.17$.

VI. Conclusion

A PWE method has been modified to include the effects of absorption and Rayleigh scattering by dust particles in an SDS. This method is applied to simulate millimeter-wave propagation in an SDS in which height profiles of particle size distribution and total number density are incorporated. Three sets of parabolic reflector with feeding horn are chosen to generate different aperture fields at 100 GHz. The height profile of PF difference at the receiving site is compared with those predicted with empirical formulas in the literature works to validate the proposed PWE method. The effects of aperture field and SDS parameters on the height profile of PF difference are then simulated and analyzed. The knowledge thus obtained is very useful to retrieve the SDS parameters with millimeter-wave signals in future studies.

References

[1] M. Akhlaq, T. R. Sheltami, and H. T. Mouftah, "A review of techniques and technologies for sand and dust storm detection," *Rev. Environ. Sci. Bio/Technol.*, vol. 11, no. 3, pp. 305–322, 2012.

[2] S. K. Satheesh, S. Deepshikha, J. Deepshikha, J. Srinvasan, and Y. J. Kaufman, "Large dust absorption of infrared radiation over Afro-Asian regions: Evidence for anthropogenic impact," *IEEE Geosci. Remote Sens. Lett.*, vol. 3, no. 3, pp. 307–311, Jul. 2006.

[3] H. M. EI-Askary, S. Sarkar, M. Kafatos, and T. A. EI-Ghazawi, "A multisensor approach to dust storm monitoring over the Nile Delta," *IEEE Trans. Geosci. Remote Sens.*, vol. 41, no. 10, pp. 2386–2391, Oct. 2003.

[4] T. Jones and S. Christopher, "Assessment of temperature and humidity changes associated with the September 2009 dust storm in Australia," *IEEE Geosci. Remote Sens. Lett.*, vol. 8, no. 2, pp. 268–272, Mar. 2011.

[5] J. Huang *et al.*, "Taklimakan dust aerosol radiative heating derived from CALIPSO observations using the Fu–Liou radiation model with CERES constraints," *Atmos. Chem. Phys.*, vol. 9, no. 12, pp. 4011–4021, 2009.

[6] Y. J. Kaufman, A. Karnieli, and D. Tanré, "Detection of dust over deserts using satellite data in the solar wavelengths," *IEEE Trans. Geosci. Remote Sens.*, vol. 38, no. 1, pp. 525–531, Jan. 2000.

[7] N. C. Hsu, S. C. Tsay, M. D. King, and J. R. Herman, "Deep blue retrievals of Asian aerosol properties during ACE-Asia," *IEEE Trans. Geosci. Remote Sens.*, vol. 44, no. 11, pp. 3180–3195, Nov. 2006.

[8] S. B. Shams and A. Mohammadzadeh, "A novel aerosol load index using MODIS visible bands: Applied to south-west part of Iran," *IEEE J. Sel. Topics Appl. Earth Observ. Remote Sens.*, vol. 8, no. 3, pp. 1167–1175, Mar. 2015.

[9] E. M. Shakshuki, T. R. Sheltami, and M. Akhlaq, "Sandstorm monitoring system architecture using agents and sensor networks," in *Proc. ACM Int. Conf. Adv. Mobile Comput. Multimedia*, New York, NY, USA, 2012, pp. 253–256.

[10] X. Y. Dong, H. Y. Chen, and D. H. Guo, "Microwave and millimeter-wave attenuation in sand and dust storms," *IEEE Antennas Wireless Propag. Lett.*, vol. 10, pp. 469–471, May 2011.

[11] Y. Li, J. Huang, and R. Yang, "The effects induced by turbulence and dust storms on millimeter waves," *Int. J. Infrared Millimeter Waves*, vol. 23, no. 3, pp. 435–443, 2002.

[12] E. M. Abuhdima and I. M. Saleh "Effect of sand and dust storms on microwave propagation signals in southern Libya," *J. Energy Power Eng.*, vol. 5, no. 12, pp. 1199–1204, 2011.

[13] A. Ahmed, A. Ali, and M. Alhaider, "Airborne dust size analysis for tropospheric propagation of millimetric waves into dust storms," *IEEE Trans. Geosci. Remote Sens.*, vol. GE-25, no. 5, pp. 593–599, Sep. 1987.

[14] M. Levy, *Parabolic Equation Methods for Electromagnetic Wave Propagation*, Inst. Eng. Technol., Herts, U.K., 2000.

[15] Z. H. Zhang, Z. Sheng, and H. Q. Shi, "Parameter estimation of atmospheric refractivity from radar clutter using the particle swarm optimization via Lévy flight," *J. Appl. Remote Sens.*, vol. 9, no. 1, 2015, Art. no. 095998.

[16] A. Ishimaru, *Wave Propagation and Scattering in Random Media*. New York, NY, USA: Academic, 1978, vol. 2, p. 259.

[17] Q. F. Dong, Y. L. Li, H. Zhang, and M. J. Wang, "Effect of sand and dust storms on microwave propagation," *IEEE Trans. Antennas Propag.*, vol. 61, no. 2, pp. 910–916, Feb. 2013.

[18] "Attenuation by atmospheric gases," ITU Recommendations, Geneva, Switzerland, p. 676-10, 2013.